

## Aqueous Proton Transfer Across Single Layer Graphene

Jennifer L. Achtyl<sup>1</sup>, Raymond R. Unocic<sup>2</sup>, Lijun Xu<sup>4</sup>, Yu Cai<sup>4</sup>, Muralikrishna Raju<sup>5</sup>, Weiwei Zhang<sup>5</sup>, Robert L. Sacci<sup>3</sup>, Ivan V. Vlassiouk<sup>3</sup>, Pasquale F. Fulvio<sup>3,6</sup>, David J. Wesolowski<sup>7</sup>, Sheng Dai<sup>7</sup>, Adri van Duin<sup>5</sup>, Matthew Neurock<sup>4</sup>, and Franz M. Geiger<sup>1\*</sup>

<sup>1</sup>Department of Chemistry, Northwestern University, 2145 Sheridan Road, Evanston, IL 60201, USA.

<sup>2</sup>Center for Nanophase Materials Sciences Oak Ridge National Laboratory, Oak Ridge, TN 37831, USA.

<sup>3</sup>Measurement Science & System Engineering Division, Oak Ridge National Laboratory, Oak Ridge, TN 37931, USA.

<sup>4</sup>Departments of Chemical Engineering and Chemistry 102 Engineers' Way, University of Virginia, Charlottesville, VA 22904-4741, USA.

<sup>5</sup>Department of Mechanical and Nuclear Engineering, Pennsylvania State University, University Park, PA 16801, USA.

<sup>6</sup>Department of Chemistry, University of Puerto Rico, Río Piedras Campus; San Juan, 00931 PR.

<sup>7</sup>Chemical Sciences Division, Oak Ridge National Laboratory, Oak Ridge, Tennessee 37831, USA.

\*Correspondence to: [geigerf@chem.northwestern.edu](mailto:geigerf@chem.northwestern.edu)

**Proton transfer across single layer graphene is associated with large computed energy barriers and is therefore thought to be unfavorable at room temperature. Experiments, however, have not yet been performed to test this prediction. Here, we subject single layer graphene on fused silica to cycles of high and low pH and show that protons transfer reversibly from the aqueous phase through the graphene to the other side where they**

**undergo acid-base chemistry with the silica hydroxyl groups. After ruling out diffusion through macroscopic pinholes, the protons are found to transfer through rare, naturally occurring atomic defect sites. Computer simulations reveal low energy processes for water-mediated proton transfer across hydroxyl-terminated atomic defect sites that participate in a Grotthuss-type relay, while defects terminated by pyrylium-like ether bridges shut down proton exchange. Unfavorable energy barriers to helium and hydrogen transfer indicate that single layer graphene is selectively permeable to aqueous protons.**

Brick-and-mortar networks of stacked graphene oxide nanosheets can act as effective membranes<sup>1-8</sup> while single layer graphene exhibits dramatically lower permeabilities towards gases<sup>4,9</sup>. In fact, graphene is thought to be unfit even for proton transfer, which is associated with computed gas phase energy barriers exceeding 1.4 eV<sup>10</sup> unless dopants or nanoscale openings are externally introduced<sup>6,7,10,11</sup>. To determine whether graphene is indeed impermeable to protons, we placed well-characterized single layer graphene prepared as previously described<sup>12</sup> on top of a fused silica substrate and cycled, at room temperature and constant ionic strength, the bulk pH of an aqueous solution above the graphene layer between basic and acidic (Supplementary Information). We tested for proton exchange through graphene by probing the underlying silica surface with an interfacial potential-dependent version of second harmonic generation (SHG, Figure 1a)<sup>13,14</sup> using 120 fsec input pulses at energies well below the graphene damage threshold<sup>12</sup>. With a detection limit of  $10^{-5}$  to  $10^{-6}$  V<sup>15</sup>, the method is sensitive enough to follow protonation or deprotonation of as little as 1% of the available silanol groups present in the area probed by SHG. The interfacial potential vanishes at the point of zero charge (PZC of fused silica  $\sim 2.5$ )<sup>16</sup> and the SHG signal intensity is small<sup>13,17,18</sup>. Increasing the pH at constant ionic strength shifts the relevant interfacial acid-base equilibria  $\text{SiOH}_2^+ + \text{OH}^- \rightleftharpoons \text{SiOH} + \text{H}_2\text{O}$  and  $\text{SiOH} + \text{OH}^- \rightleftharpoons \text{SiO}^- +$

H<sub>2</sub>O (pKa ~4.5 and ~8.5)<sup>13,17,19</sup> to the right and the resulting interfacial potential polarizes the interfacial water molecules such that the SHG signal intensity increases<sup>13,17</sup>. Intuitively, the close proximity of the graphene layer and the charged fused silica surface, combined with the sensitivity of the method, make our approach akin to an Å-scale voltmeter for detecting even rare occurrences of proton exchange.

As shown in Figure 1b, we find no significant difference between the SHG vs. time traces recorded in the presence and absence of graphene, and no statistically significant differences in the kinetic rates and jump durations (Supplementary Information). The SHG responses to pH changes are consistent with the acid-base equilibria of the fused silica/water interface<sup>13,14,18,20</sup>, indicating the SHG experiments do not track merely ion adsorption to the graphene/water interface but acid-base chemistry at the fused silica surface underneath it, for which proton transfer across the membrane is a necessary condition (Supplementary Information). As expected from refs 1-5, porous graphene multilayers do not inhibit proton transfer either (Supplementary Information).

Scanning electron microscopy (SEM) images of graphene single layers deposited on fused silica windows show a low density of macroscopic pinholes and that the graphene is free of cracks or folds (Figure 1c). Using 2D proton diffusion coefficients that account for proton trapping<sup>21,22</sup> by the surface silanol groups<sup>23,24</sup>, we estimate (Supplementary Information) a 4% to 21% likelihood of focusing the 30 µm diameter laser beam onto an area that is subject to two-dimensional proton diffusion around a given pinhole. Additional computer simulations reveal (Supplementary Information) slow water-self diffusion and a strongly enhanced local water structure at high pH near the silica surface, and fast protonation of surface SiO<sup>-</sup> groups, indicating negligible 2D proton mobility under basic conditions. The diffusion of protons from

the few macroscopic pinholes that are present in our samples, or, alternatively, from the sample edge, to the area probed by the laser can therefore not explain our observations of proton transfer through graphene.

Scanning transmission electron microscopy (STEM) was then used to search for atomic defects using annular dark field (ADF) STEM imaging at 60 kV. The majority of the images show perfect six-fold symmetry in the position of the carbon atoms and vast areas that lack grain boundaries and atomic, or vacancy, defects (Figure 1d). Nevertheless, similar to prior reports of atomic scale vacancy point defects<sup>25,26</sup>, we find, albeit rarely, atomic defects (Figure 1e). These defects could originate from the synthesis process or cosmic rays, as the STEM experiments are carried out below the knock-on damage threshold for graphene<sup>27</sup>, while the femtosecond laser pulses are attenuated below the onset of processes other than SHG<sup>12</sup>.

We then used density functional theory (DFT) calculations (Figure 2) and ReaxFF reactive force field molecular dynamics (Figure 3)<sup>28-30</sup>, respectively, to elucidate the mechanisms for proton transfer. DFT simulations track the detailed changes in the electronic structure and quantify corresponding activation barriers as protons transfer from the water layer through the graphene interface and exit into solution on the opposite side of the surface, whereas the ReaxFF simulations provide a more detailed representation of the interfaces and more rigorous accounting of the dynamics. The barrier to proton transfer through graphene was calculated to decrease from over 3.0 eV to under 1.0 eV in the presence of atomic scale defect sites (Table S4). The simulations indicate that the proton transfers from the solution phase to the surface through the center of the defect site and into the solution on the opposite side of the membrane via a Grotthuss<sup>31</sup> mechanism involving proton shuttling. The solution phase proton shuttling

paths occur with barriers of  $< 0.2$  eV whereas the barrier to transfer through a given defect site is somewhat higher due to limited access of water and OH groups required for proton shuttling.

The quad vacancy site is found to be the smallest defect site that facilitates proton transfer through graphene (Table S4). This site is comprised of 6 coordinatively unsaturated carbon atoms that are either terminated with 3 oxygen atoms in epoxide-like arrangements reminiscent of pyrylium cations, or with 6 hydroxide groups. Proton transfer through the pyrylium-terminated 4V site requires 1.7 eV (Figure 2A), which we attribute to the protophobicity of pyrylium cations and their in-plane localization, which leaves a 3.4 Å gap between water and the graphene substrate that prevents proton transfer. The hydroxyl-terminated site, however, provides hydrogen bonding conduits via a Grotthuss mechanism that lowers the barrier to proton transfer to just 0.68 eV (Figure 2B), indicating it will occur at room temperature. ReaxFF simulations shows that a water channel, which establishes itself upon proton transfer, thins and finally vanishes when the pairs of OH groups terminating the defect site are successively replaced with oxygen atoms (Figure 3A-D). These transfer paths are selective to aqueous protons as helium and H<sub>2</sub> transfer requires barriers exceeding 1.9 eV (Supplementary Information).

We conclude that aqueous protons transfer through single layer graphene via rare, OH-terminated atomic defects. From the SHG signal jump rates and the times required for 2D proton diffusion, we estimate that just one atomic defect in the 30 μm laser spot is enough to allow for the apparent unimpeded protonation and deprotonation of the interfacial silanol groups. While the rarity of the atomic defect sites would make it challenging to follow proton exchange across graphene using pH-sensitive electrodes, the close proximity of the graphene layer and the charged fused silica surface, where the experimental observation of surface protonation and

deprotonation is made by SHG, allows for the experimental observation of proton exchange across these rare defects. The identification of low barriers specifically for water-assisted transfer of protons through OH-terminated atomic defects in graphene, and high barriers for oxygen-terminated defects could be an important step toward the preparation of zero-crossover proton-selective membranes.

**Acknowledgments:** This work was supported by the Fluid Interface Reactions, Structures and Transport (FIRST) Center, an Energy Frontier Research Center funded by the U.S. Department of Energy, Office of Science, Office of Basic Energy Science.

## References and Notes:

- 1 Joshi, R. K. *et al.* Precise and Ultrafast Molecular Sieving Through Graphene Oxide Membranes. *Science* **343**, 752-754 (2014).
- 2 Mi, B. Graphene Oxide Membranes for Ionic and Molecular Sieving. *Science* **343**, 740-742 (2014).
- 3 Gao, W. *et al.* Ozonated Graphene Oxide Film as a Proton-Exchange Membrane. *Angew. Chemie Int. Ed.* **53**, 1-6 (2014).
- 4 Nair, R. R., Wu, H. A., Jayaram, P. N., Grigorieva, I. V. & Geim, A. K. Unimpeded Permeation of Water Through Helium-Leak-Tight Graphene-Based Membranes. *Science* **335**, 442-444 (2012).
- 5 Guo, F. *et al.* Graphene-based environmental barriers. *ES&T* **46**, 7717-7724 (2012).
- 6 Hauser, A. W. & Schwerdtfeger, P. Nanoporous Graphene Membranes for Efficient  $^3\text{He}/^4\text{He}$  Separation. *J. Phys. Chem. Lett.* **3**, 209-213 (2011).
- 7 Banerjee, S. *et al.* Electrochemistry at the Edge of a Single Graphene Layer in a Nanopore. *ACS Nano* **7**, 834-843 (2013).
- 8 Wang, X. D. *et al.* Atomistic Origins of High Rate Capability and Capacity of N - Doped Graphene for Lithium Storage. *Nano Lett.* **14**, 1164-1171 (2014).
- 9 Bunch, J. S. *et al.* Impereable Atomic Membranes from Graphene Sheets. *Nano Lett.* **8**, 2458-2462 (2008).
- 10 Miao, M., Nardelli, M. B., Wang, Q. & Liu, Y. First principles study of the permeability of graphene to hydrogen atoms. *PCCP* **15**, 16132-16137 (2013).
- 11 Jiang, D., Cooper, V. R. & Dai, S. Porous graphene as the ultimate membrane for gas separation. *Nano Lett.* **9**, 4019-4024 (2009).
- 12 Achtyl, J. L. *et al.* Free Energy Relationships in the Electrical Double Layer over Single-Layer Graphene. *J. Am. Chem. Soc.* **135**, 979-981 (2013).
- 13 Ong, S., Zhao, X. & Eissenthal, K. B. Polarization of water molecules at a charged interface; second harmonic studies of the silica/water interface. *Chem. Phys. Lett.* **191**, 327-335 (1992).
- 14 Gibbs-Davis, J. M., Kruk, J. J., Konek, C. T., Scheidt, K. A. & Geiger, F. M. Jammed Acid-Base Chemistry at Interfaces. *J. Am. Chem. Soc.* **130**, 15444-15447 (2008).
- 15 Konek, C. T. *et al.* Interfacial Acidities, Charge Densities, Potentials, and Energies of Carboxylic Acid-Functionalized Silica/Water Interfaces Determined by Second Harmonic Generation. *J. Am. Chem. Soc.* **126**, 11754-11755 (2004).
- 16 Stumm, W. & Morgan, J. J. *Aquatic Chemistry, Chemical Equilibria and Rates in Natural Waters*. 3rd edn, (John Wiley & Sons, 1996).
- 17 Higgins, S. R., Stack, A.G., Knauss, K.G., Eggleston, C.M., Jordan, G. Probing molecular-scale adsorption and dissolution-growth processes using nonlinear optical and scanning probe methods suitable for hydrothermal applications. *Geochemical Society Special Publication No. 7*, 111 (2002).
- 18 Azam, M. S., Weeraman, C. N. & Gibbs-Davis, J. M. Halide-Induced Cooperative Acid-Base Behavior at a Negatively Charged Interface. *J. Phys. Chem. C* **117**, 8840-8850 (2013).

- 19 Duval, Y., Mielczarski, J. A., Pokrovsky, O. S., Mielczarski, E. & Ehrhardt, J. J. Evidence of the Existence of Three Types of Species at the Quartz-Aqueous Solution Interface at pH 0-10: XPS Surface Group Quantification and Surface Complexation Modeling. *J. Phys. Chem. B*. **106**, 2937-2945 (2002).
- 20 Stack, A. G., Higgins, S. R. & Eggleston, C. M. Point of zero charge of a corundum-water interface probed with optical second harmonic generation (SHG) and atomic force microscopy (AFM): New approaches to oxide surface charge. *Geochim. Cosmochim. Acta* **65**, 3055-3063 (2001).
- 21 Petersen, M. K. & Voth, G. A. Characterization of the Solvation and Transport of the Hydrated Proton in the Perfluorosulfonic Acid Membrane Nafion. *J. Phys. Chem. B*, 18594-18600 (2006).
- 22 Junge, W. & McLaughlin, S. The role of fixed and mobile buffers in the kinetics of proton movement. *Biochim Biophys Acta*. **890**, 1-5 (1987).
- 23 Eikerling, M., Kornyshev, A. A., Kuznetsov, A. M., Ulstrup, J. & Walbran, S. Mechanisms of Proton Conductance in Polymer Electrolyte Membranes. *J. Phys. Chem. B* **105**, 3646-3662 (2001).
- 24 Choi, P., Jalani, N. H. & Datta, R. Thermodynamics and Proton Transport in Nafion II. Proton Diffusion Mechanisms and Conductivity. *J. Electrochem. Soc.* **152**, E123-E130 (2005).
- 25 Hashimoto, A., Suenaga, K., Gloter, A., Urita, K. & Iijima, S. Direct evidence for atomic defects in graphene layers. *Nature* **430**, 870-873 (2004).
- 26 Meyer, J. C. *et al.* Direct Imaging of Lattice Atoms and Topological Defects in Graphene Membranes. *Nano Lett.* **8**, 3582-3586 (2008).
- 27 Meyer, J. C. *et al.* Accurate Measurement of Electron Beam Induced Displacement Cross Sections for Single-Layer Graphene. *Phys. Rev. Lett.* **108**, 196102 (2012).
- 28 Kresse, G. & Furthmuller, J. Efficient iterative schemes for ab initio total-energy calculations using a plane-wave basis set. *Phys. Rev. B* **54**, 11169-11186 (1996).
- 29 van Duin, A. C., Dasgupta, S., Lorant, F. & Goddard, W. A. ReaxFF: A Reactive Force Field for Hydrocarbons. *J. Phys. Chem. A* **105**, 9396-9409 (2001).
- 30 Baustian, K. J. *et al.* Importance of aerosol composition, mixing state, and morphology for heterogeneous ice nucleation: A combined field and laboratory approach. *Journal Of Geophysical Research-Atmospheres* **117**, doi:D06217 10.1029/2011jd016784 (2012).
- 31 de Grotthuss, C. J. T. Sur la décomposition de l'eau et des corps qu'elle tient en dissolution à l'aide de l'électricité galvanique. *Ann. Chim.* **58**, 54-73 (1806).



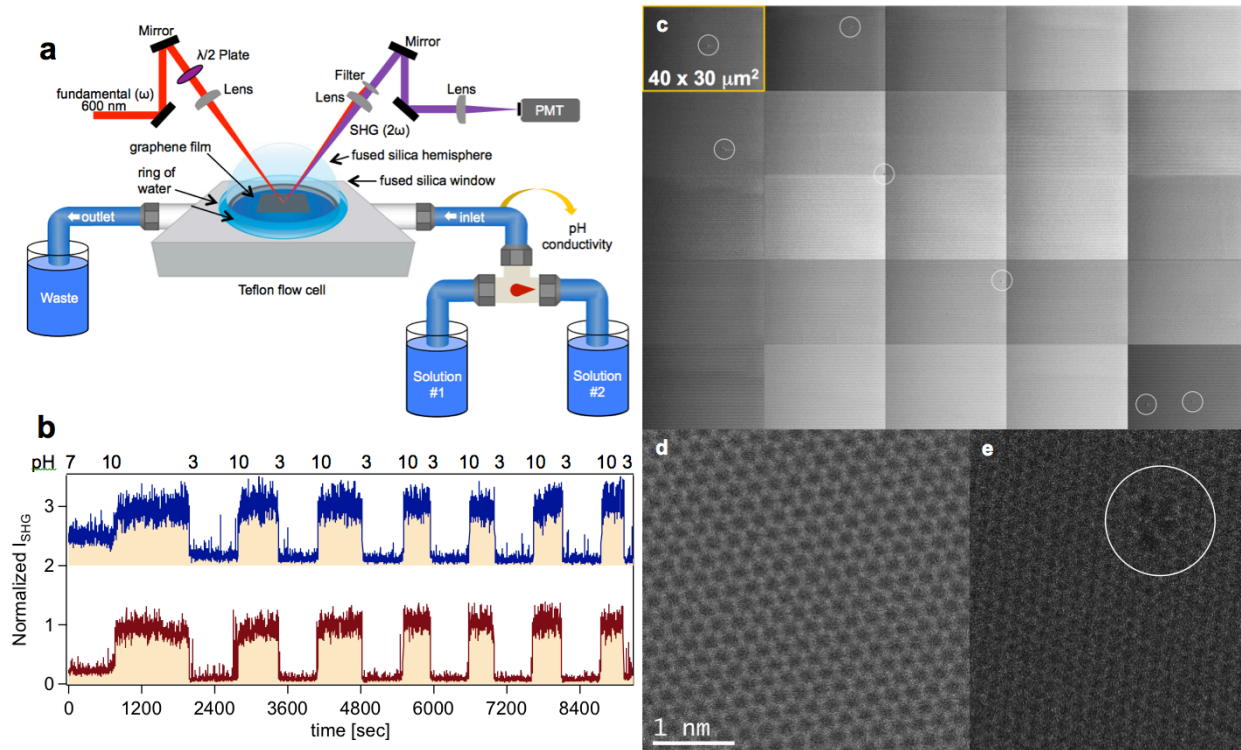


**Fig. 1.** (A) Experimental setup using a waveplate ( $\lambda/2$ ) to prepare 600 nm light plane-polarized parallel to the plane of incidence (p-in) while a photomultiplier tube (PMT) detects the second harmonic generation photons at  $\lambda=300$  nm. (B) p-in/all-out Polarized SHG E-field recorded as a function of time from the fused silica/water interface during pH jumps from 7 to 3 to 10 and subsequent pH cycling between 3 and 10 at a bulk aqueous flow of 0.9 mL/sec and 1 mM NaCl concentration in the absence (crimson, bottom) and presence (blue, top) of single layer graphene placed between the fused silica substrate and the flowing bulk aqueous phase. (C) Composite of 25 SEM images of single layer graphene on a fused silica substrate, showing 7 macroscopic pinholes, marked by white circles. (D) High resolution aberration-corrected ADF STEM images of defect-free single layer graphene on a TEM grid and (E) of a rarely imaged atomic defect.

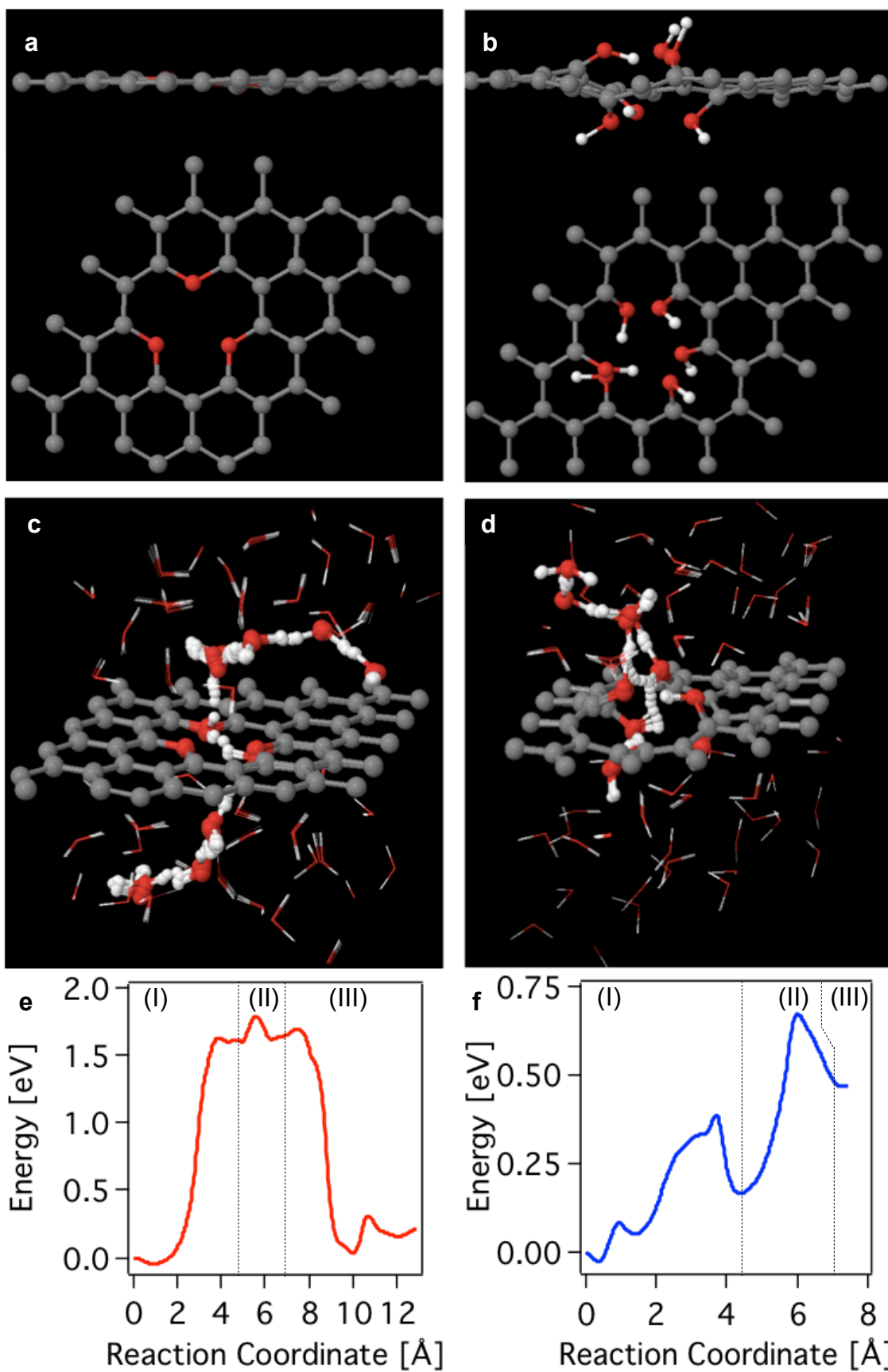


**Fig. 2.** Side and top views of oxygen- (**A**) and OH-(**B**) terminated defect models used in the DFT calculations. Snapshots (**C**, **D**) and energetics (**E**, **F**) from the nudged elastic band calculations for proton transfer through the ether- and OH- terminated defect sites marking (**region I**) release of proton from  $\text{H}_3\text{O}^+$  to ether and OH group, respectively; (**region II**) relay of proton between ether and OH groups, respectively; (**region III**) release of proton from ether and OH groups to  $\text{H}_3\text{O}^+$ , respectively. Denotations of spheres: grey=carbon; red=oxygen; white=hydrogen atoms.

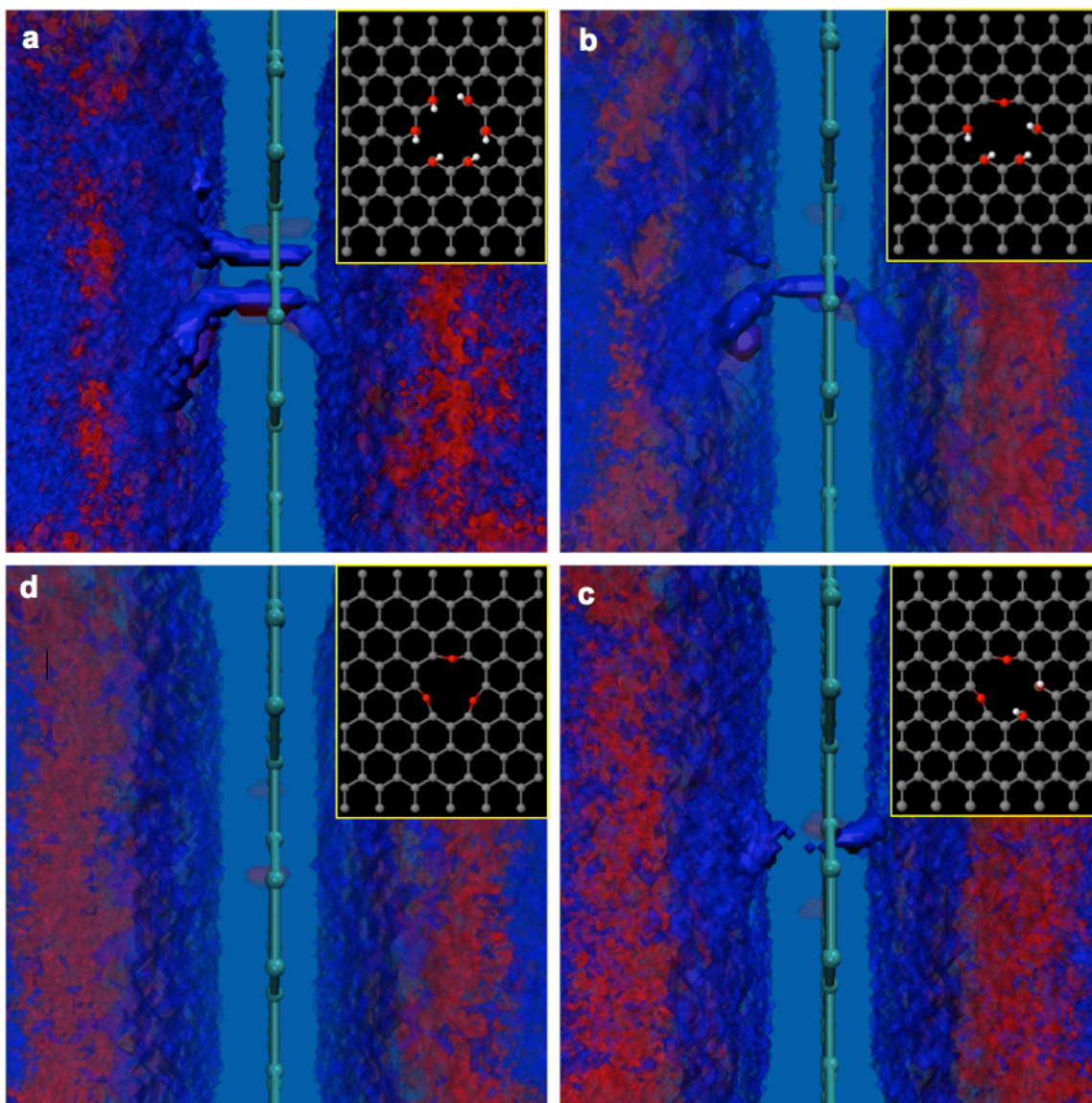


**Fig. 3.** Water channel formation from ReaxFF calculations of water mediated proton transfer through atomic defects terminated in 6 OH groups (A), 4 OH groups and one oxygen atom (B), 2 OH groups and two oxygen atom (C), and three oxygen atoms (D). Denotations of spheres: grey=carbon; red=oxygen; white=hydrogen atoms.

2518 words.

**Supplementary Materials:**

Materials and Methods, and control studies, Figures S1-S21, Tables S1-S5. Information on materials and methods is available upon request by emailing the corresponding author.